Revue de micropaléontologie 70 (2021) 100480

Contents lists available at ScienceDirect

Revue de micropaléontologie

journal homepage: www.elsevier.com/locate/revmic

Micro/Strat Eastern Medit Special Issue

Reconstruction of oceanographic and environmental conditions in the eastern Mediterranean (Kottafi Hill section, Cyprus Island) during the middle Miocene Climate Transition

M. Athanasiou [a], M.V. Triantaphyllou [a,*], M.D. Dimiza [a], A. Gogou [b], I. Panagiotopoulos [b], A. Arabas [c], E. Skampa [a], K. Kouli [a], M. Hatzaki [a], E. Tsiolakis [d]

[a] National and Kapodistrian University of Athens, Faculty of Geology and Geoenvironment, Panepistimioupolis 15784, Athens, Greece
[b] Hellenic Centre for Marine Research, Institute of Oceanography, 190 13 Anavyssos, Attiki, Greece
[c] Institute of Geological Sciences, Polish Academy of Sciences, Research Centre in Kraków, ul. Senacka 1, Kraków 31-002, Poland
[d] Geological Survey Department of Cyprus, 1 Lefkonos Street, 2064 Strovolos, Lefkosia, Cyprus

ARTICLE INFO

Keywords:
Carbonate succession
Sapropelic layers
Calcareous nannofossils
Oxygen/carbon isotopes
Palynomorphs
middle Miocene Mi-events

ABSTRACT

The multi-proxy investigation of the deep-marine Kottafi Hill section (KHS), a part of the carbonate system of the Miocene Pakhna Formation, Cyprus, involved such proxies as calcareous nannofossil analysis, measurements of the oxygen and carbon isotope composition of the planktonic foraminifer *Orbulina universa*, and determination of the pollen and palynomorph contents, revealed the importance of these sedimentary sequences in the assessment of the impact of major global events during the middle Miocene on the regional scale. The KHS spans the 20.89–11.6 Ma time interval, during which eighteen OC-rich siltstone intercalated laminae have been deposited under warm and humid climate at 15.5–11.6 Ma. These layers can be possibly considered as the precursors of sapropelic layers mostly developed in the eastern Mediterranean Basin during Pliocene–Holocene. The global glacial events Mi3a–Mi5, traced by $\delta^{18}O$ planktonic foraminifera records in the KHS, represent the stepwise cooling phase during the middle Miocene Climate Transition.

1. Introduction

As stated in IPCC reports (e.g., IPCC, 2013), reconstructions from paleoclimatic archives would be informative on the climate system functioning in the past, before the human spread, and thus useful for the understanding of the current trend towards a warmer future.

An interesting interval in the Cenozoic climatic history is the Miocene Climatic Optimum (MCO; c.a. 14.7–17.0 Ma), featured by sustained global warmth and reduced continental ice volume (e.g., Zachos et al., 2001; Brandano, 2017). The MCO followed a long period of 24 million years where CO_2 estimations remained to pre-industrial levels (Pagani et al., 2005; Burke et al., 2018; Westerhold et al., 2020). In contrast, proxy data imply CO_2 concentrations of 400–600 ppm during MCO (Kurschner and Kvacek, 2009), and SST reconstructions indicate an average surface temperature between 3–5 °C above pre-industrial levels (Flower, 1999). The MCO is recorded within a long-term positive carbon isotope shift, known as the Monterey Carbon Isotope Excursion. This prolonged positive carbon isotope excursion (~13.5–17.0 Ma) is associated with extensive organic rich deposits (i.e., California Monterey Formation) and is featured by six carbon isotope maxima (CM1-CM6), in pace with the 400 kyr eccentricity cycle (Woodruff and Savin, 1991; Holbourn et al., 2007; Brandano et al., 2017). Post-dating MCO, the climate experienced a stepwise cooling, the middle Miocene Climate Transition (mMCT), which led to the rapid expansion of the East Antarctic ice sheet at ~13.8 Ma (Miller et al., 1991; Flower and Kennett, 1994; Zachos et al., 2001). During the mMCT, several oxygen isotope positive shifts (Mi3-Mi5 events; Miller et al., 1991; Turco et al., 2001; Quaijtaal et al., 2014) represent a series of brief glaciations indicating a drop in the sea bottom water temperature and/or an increase in the ice volume. The middle Miocene cooling is characterized by an initialrelatively small shift at 14.2 Ma and a second major shift at 13.8 Ma (Mi3a and Mi3b isotopic events respectively; Shevenell et al., 2004), associated with a shift to heavier benthic foraminiferal $\delta^{13}C$ values that coincides with the CM6 event (Woodruff and Savin, 1991).

The semi-enclosed, well ventilated Mediterranean basin is considered as a unique physical model for the observation of the climate changes throughout the geologic timescale (e.g., Béthoux, 1993). Major high-latitude atmospheric teleconnections appear to affect the Mediterranean's climate on multi-decadal to centennial timescales, presenting large temporal variability and strong seasonal cycles (e.g., Béthoux, 1993). For

* Corresponding author.
E-mail address: mtriant@geol.uoa.gr (M.V. Triantaphyllou).

http://doi.org/10.1016/j.revmic.2020.100480

instance, Marullo et al. (2011) and Mariotti and Dell'Aquila (2012) argue about the existence of a close relationship between the Atlantic Multi-Decadal Oscillation (AMO) and the Mediterranean's SSTs on decadal timescales, while Skliris et al. (2012) have shown that the recent warming trend demonstrated by the Mediterranean's surface waters is highly correlated with both the Eastern Atlantic SST pattern and the AMO index. In contrast to the modern oceanographic conditions, enhanced freshwater discharges induced by the insolation-controlled intensification of the African monsoon, notably through the Nile River (e.g., Rossignol-Strick, 1985; Rohling, 1994), resulted to the sensitive response of the eastern Mediterranean hydrographic regime. Thus, the ~23 kyr precession periodicity has led to an episodic deposition of multiple organic-rich layers, so-called sapropels, exhibiting an age ranging from late Miocene to modern times (e.g., Hilgen et al., 2003; Rohling et al., 2015; Athanasiou et al., 2017). Sapropel formation is associated with increased freshwater inputs delivering nutrients in the basin and concomitant enhanced stratification (e.g., Giunta et al., 2003; Gogou et al., 2007; Triantaphyllou et al., 2009, 2016), resulting to a productive lower photic zone and dysoxic/anoxic conditions in the bottom of the basin supporting organic matter preservation (e.g., Rossignol-Strick, 1985; Rohling, 1994; Emeis et al., 2000; Casford et al., 2003; De Lange et al., 2008).

Sapropelic layers have been reported from the central Mediterranean sporadically during the late Miocene (e.g., Nijenhuis et al., 1996; Negri et al., 1999; Sierro et al., 2003; Abels et al., 2005), whereas only one site has been reported in the eastern Mediterranean (Taylforth et al., 2014). In addition, a few on land sites display continuous sapropelic marine successions spanning the mMCT, i.e., Malta and Gozo islands (Sprovieri et al., 2002; John et al., 2003; Mourik et al., 2011) and the astronomically dated La Vedova Beach section located in central Mediterranean (Hüsing et al., 2010; Mourik et al., 2010). However, the existing carbon isotope curves during the MCO in the Mediterranean region, are either characterized by low resolution (Kocsis et al., 2008) or by being poorly age-constrained (Reuter et al., 2013; Auer et al., 2015).

Calcareous nannofossils have been rapidly evolved through geological time providing numerous fossil indices used as biostratigraphic tools; the group is also responding quickly to changes in environmental conditions providing a useful means for palaeoceanographic reconstructions (e.g., Flores et al., 2005; Di Stefano et al., 2015; Triantaphyllou et al., 2009, 2016; Athanasiou et al., 2015, 2017). In addition, shifts in the terrestrial environment (i.e., changes in vegetation, erosion events) characterize the pollen and palynomorph assemblages (e.g., Kouli et al., 2012). Carbon isotope values of marine calcite from microfossil tests (e.g., foraminifera) are suitable for understanding changes in organic marine productivity, ocean circulation patterns (vertical mixing and stratification in the water column) and general carbon cycle changes associated with the exchange of CO_2 between the ocean and atmosphere, while changes in their oxygen isotopic composition may serve as a basis for the paleotemperature interpretation, estimation of the ice volume and salinity variations (e.g., Turco et al., 2001; Sierro et al., 2003; Abels et al., 2005; Mourik et al., 2011).

The Kottafi Hill section (KHS; Pakhna Formation) on Cyprus Island represents a lower to middle Miocene well-exposed sequence of hemipelagic chalky-marly deposits. Preliminary results of the calcareous nannofossil biostratigraphy of the KHS (Athanasiou et al., 2013) indicated that it represents a promising sedimentary archive for the

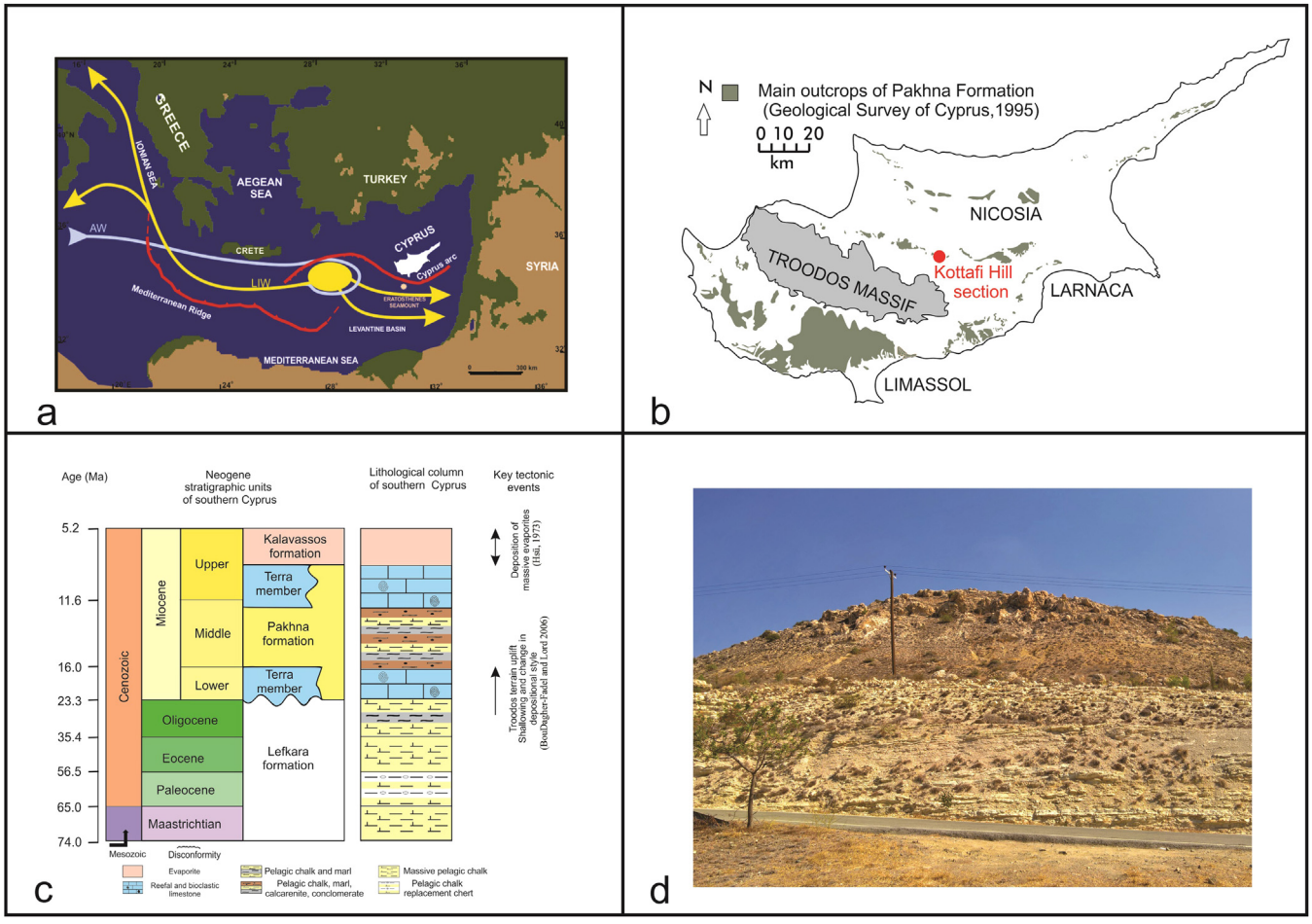

Fig. 1. (a) Location of Cyprus Island in the context of eastern Mediterranean Sea and northern Levantine Sea (AW: Atlantic Water, LIW: Levantine Intermediate Water), **(b)** Simplified geological map of Cyprus focusing on the sediments of Pakhna formation. **(c)** Generalized lithostratigraphy and chronostratigraphy of southern Cyprus stratigraphic units and the main tectonic events (modified from Manzi et al., 2014, after Robertson et al., 1991) **(d)** Kottafi Hill section.

investigation of potential sapropelic layers in the eastern Mediterranean during the mMCT.

The present study aims (a) to establish a solid biostratigraphic framework for the KHS sedimentary sequence, (b) to apply a multi-proxy approach (i.e., calcareous nannofossil assemblages, palynomorph concentrations and stable isotope composition of planktonic foraminifera), in order to investigate the paleoceanographic and paleoclimatic conditions under which the eastern Mediterranean sapropelic layers begun to form and (c) to determine the impact of the major global cooling events on the eastern Mediterranean during the mMCT.

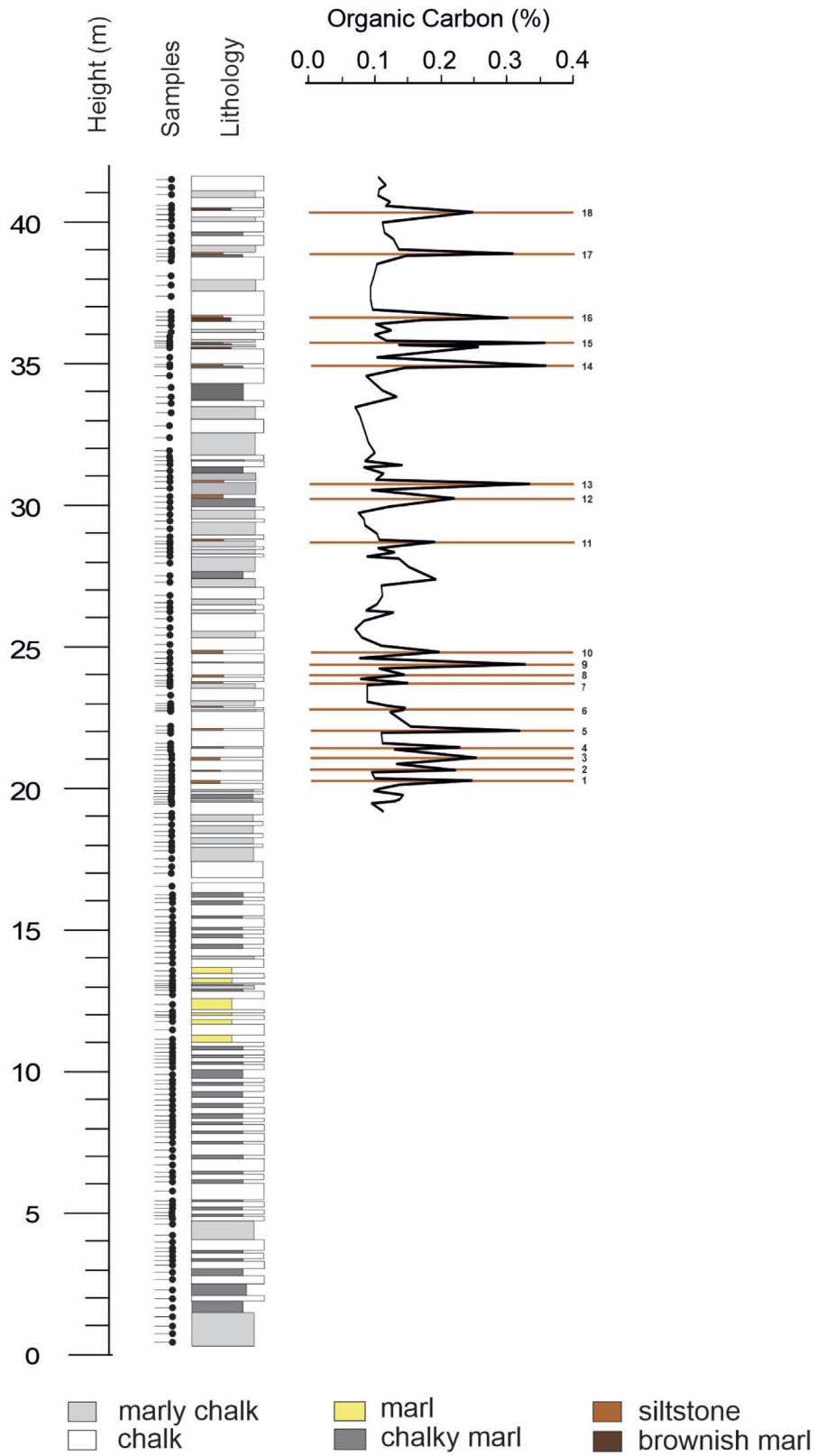

Fig. 2. Lithology, detailed logging of Kottafi Hill sediments and Total Organic Carbon content (TOC%) for the 17–42 m interval. TOC peaks correspond to the laminated siltstone layers (1-18), highlighted in brown bands.

2. Study area: the Kottafi Hill section on Cyprus Island

Located in the Levantine Basin, Cyprus Island is considered as part of a northward-dipping subduction zone (Cyprean Arc) that extends between southern Cyprus and the Eratosthenes Seamount (Fig. 1a), on the northern margin of the African Plate (Payne and Robertson, 1995; Harrison et al., 2004). During late Oligocene to early Miocene, a basement uplift of the Troodos Terrane caused shallowing and fundamental environmental changes (BouDagher-Fadel and Lord, 2006). These processes led to the deposition of the deep-marine biogenic sediments of the Lefkara Formation and the overlying early-late Miocene hemipelagic sequence of the Pakhna Formation, widely outcropping in southern Cyprus, northwest of Limassol (Fig. 1b, c). The latter consists of marine carbonate sediments with distinct cyclicity (i.e., marl, chalky marl, marly chalk and chalk; Fig. 1c), deposited in tectonically-controlled shallow to deep-marine settings (Smith and Gale, 2009). Up to now, several sections of the Pakhna Formation have been studied (e.g., Lord et al., 2009; Smith and Gale, 2009; Taylforth et al., 2014), still with poor biostratigraphic documentation (e.g., Mantis, 1970; Hadjistavrinou, 1974; Davies, 2001).

The KHS is a 42.1-meter-thick succession located in the outer part of the Nicosia region (Fig. 1b, d) and represents a well-exposed complete sequence of the hemipelagic Pakhna Formation. The sediments comprise alternating hemipelagic carbonates and intercalated allochthonous laminated siltstone layers. The carbonates include (Fig. 2): (i) deep-water white foraminiferal limestone (prevailing between 19–27 m and 34–42 m), which has less than 5 dry weight (dw) % of terrestrial clay and consists of coccolith ooze with planktonic foraminifera; (ii) white foraminiferal marly chalk (between 17–19 m and 27–33 m) containing ~10 dw% of terrigenous clay; (iii) chalky marls and marl facies (mostly occupying the lower part of the section), which are composed of up to ~30 dw% of land-derived clay. Finally, eighteen laminated siltstone layers (3–12 cm thick) are present throughout the middle and upper part of the section (above 20.4 m), displaying dark brown colour and extremely poor cementation, which imply rapid clastic sedimentation. A more detailed description of the carbonate facies occurring in KHS is presented in Davies (2001).

3. Methods

3.1. Sampling and spectral analysis

Sampling resolution involved a range between 5 cm–30 cm and it was performed throughout the sedimentary sequence in KHS for a total number of 198 samples; one to three samples have been taken from each bed depending on the bed thickness (Fig. 2).

Following the methodology of Mitchel et al. (2008), the lithological log has been converted to a numerical string, assigning a value from 0 to 255 to each layer of the section, i.e. from chalk to siltstone, according to the colour of the beds. Spectral analysis has been performed on the produced lithology numerical string with the Lomb Normalized Periodogram for unevenly sampled data (Press et al., 1992), testing the hypothesis that the population represents a significant periodic signal against the random noise.

3.2. Total organic carbon analysis

Total organic carbon (TOC) content was measured in 104 dry-freezed and homogenized samples from the upper part of KHS (19.74–38.92 m). Samples were initially de-carbonated using repetitive additions of HCl (25%, v/v) and separated by 60 °C drying steps, until no effervescence was observed. Measurements were carried out at the laboratories of the Institute of Oceanography, Hellenic Centre for Marine Research, Greece, using an elemental analyzer (Fisons EA-1108 CHN), following the procedures described by Verardo et al. (1990). The precision of the method was within 5%.

3.3. Foraminiferal analysis

One hundred and thirty samples (~10 g each) taken accross the the entire KHS sequence were soaked in a hydrogen peroxide solution (30%), ultra-sonicated and sieved using a 125 μm mesh. A total amount of 300 planktonic foraminifera and the corresponding content of benthic foraminiferal specimens were collected per treated sediment sample. The planktonic foraminiferal assemblages have been assessed in order to detect the exact position of the species *Orbulina universa* first occurrence (FO) in the sedimentary sequence (*O. universa* FO; Lirer et al., 2019).

3.4. Calcareous nannofossil analysis

The samples for the calcareous nannofossil (CN) analysis were prepared according to standard smear slide techniques (Bown and Young, 1998) and were examined using a Leica DMLSP polarising Light Microscope (LM) under 1250× working magnification. A Jeol JSM 6360 Scanning Electron Microscope (SEM) was used for taxonomical purposes.

The biostratigraphic frame was based on the analysis of calcareous nannofossil marker taxa in 80 samples from the entire KHS sedimentary sequence, by counting the index species in a predetermined number of taxonomically related forms (Fornaciari and Rio, 1996; Fornaciari et al., 1996). This method was applied for the evaluation of the main biostratigraphic indices relative abundance, such as *Helicosphaera carteri, H. euphratis, H. ampliaperta* (approx. 100 *Helicosphaera* specimens); *Sphenolithus belemnos, S. heteromorphus* (approx. 100 *Sphenolithus* specimens); *Discoaster kugleri, D. signus* (approx. 100 *Discoaster* specimens), while the counting of the *Calcidiscus premacintyrei* forms was performed relative to 50 *Calcidiscus* specimens. Data are presented as relative abundances. The zonal assignment for the KHS record follows the biostratigraphic scheme of Agnini et al. (2017) that incorporates Backman et al. (2012) and is correlated to Martini (1971) biozones. The numerical ages of the CN biohorizons and biozone boundaries are given according to Agnini et al. (2017).

In order to reconstruct the palaeoceanographic conditions prevailing during the deposition of the upper part of the KHS (19.74–38.92 m) that contains the siltstone layers, the total calcareous nannofossil assemblage composition was analysed in 63 samples with average sample resolution of 50 cm. All nannofossil taxa were counted taking into account at least 500 nannofossil specimens (e.g., Fornaciari and Rio, 1996; Athanasiou et al., 2015). Counts in additional 15 fields of view have been performed for the less common taxa such as *Syracosphaera* spp. and *Rhabdosphaera* spp. (e.g., Giunta et al., 2003; Triantaphyllou et al., 2009). *Coccolithus* spp. and *Calcidiscus* spp. were plotted together as they both present ecological affinities to cool mesotrophic waters (e.g., Haq, 1980; Hagino and Okada, 2006; Bolton, 2010).

3.5. Palynological analysis

Palynological analysis was performed on 40 samples from the middle-upper part of the sequence (19.74–38.92 m). Approximately 5 g of each sample were successively treated with HCl (36%), HF (38%) and KOH (10%), following standard preparation methods for palynological samples (Faegri and Iversen, 1989). The samples were then sieved through a 10 μm sieve and the residues were stored and mounted in glycerine. Microscopic analysis was performed at 400× magnification and all terrestrial and aquatic palynomorphs, including pollen and spores, fungal remains, green algae cysts and microscopic charcoal, were identified and counted. A mean terrestrial pollen and spore sum of 200 grains per sample was reached in most of the samples studied, while 11 samples that have not reached the threshold of 150 pollen and spore grains were considered barren and excluded from this study. The palynomorph content was calculated as grains/g of dry sediment based on the known quantity of exotic spores, namely *Lycopodium* tablet,

introduced at the first step of the chemical processing (Faegri and Iversen, 1989).

3.6. Stable isotope analysis

The carbon and oxygen isotope composition analyses were performed on the planktonic foraminifer *Orbulina universa,* in 63 samples. Six specimens per sample were hand-picked and cleaned in an ultrasonic bath for 3–5 s at a frequency of 40 kHz, to remove adhering sediment particles. Measurements were carried out in the Stable Isotope Laboratory of the Department of Earth and Planetary Sciences in the University of California, Davis, using NBS-19 calcite standard. The carbon and oxygen isotope ratios are reported using the delta notation (δ) in ‰, relative to the Vienna Pee Dee Belemnite international standard (VPDB). The measurement precision of the $^{18}O/^{16}O$ ratio was ±0.04‰ and ±0.03‰ of the $^{13}C/^{12}C$ ratio.

4. Results

4.1. Total organic carbon

In the studied interval of the KHS (~20–40 m), the TOC content varied from 0.07 to 0.36% (average 0.25%; Fig. 2). The highest concentration of the TOC was observed within the thin siltstone layers (up to 0.36%), while in the chalky/chalky marly layers the TOC content was less than 0.15% (average 0.11%).

4.2. Foraminiferal assemblages

Foraminifera shells were present throughout the whole KHS, however, their preservation state varied from moderate to poor. The best-preserved tests were observed in the siltstone laminated layers while the poorest (mostly recrystallized) specimens dominated the chalky layers. All analysed samples were composed of planktonic foraminifera (>95%). The first representatives of the species *Orbulina universa* have been observed at 22.89 m (Fig. 3a). Few specimens of the benthic taxa *Cibicides* and *Hoeglundina* have been detected in the chalky marls, while the siltstone layers displayed sporadic individuals of the infaunal *Bolivina* spp. and *Uvigerina* spp.

4.3. Calcareous nannofossils

4.3.1. Biostratigraphy and age model

The CN biostratigraphic analysis revealed several biohorizons (Agnini et al., 2017) within the KHS sedimentary record (Fig. 3a). The turnover in dominance of *H. carteri* (max. >60%) over *H. euphratis* was observed 1.70 m above the base of the section, marking the base of biozone CNM4 (Backman et al., 2012; Agnini et al., 2017). Upwards, the B of *H. ampliaperta* (20.43 Ma) was recognised at 3.20 m in the lower part of CNM4. The B of *S. belemnos* was observed at 5.28 m (19.01 Ma at the base of CNM5) and the Bc of *S. heteromorphus* (17.75 Ma) was defined at 7.71 m, marking the base of biozone CNM6. The B of *D. signus* was recorded at 15.21 m; the T of *S. heteromorphus* biohorizon at 33.22 m points to 13.53 Ma, approximating the Langhian/Seravallian (NN5/NN6 and CNM7/CNM8) boundary (Fornaciari et al., 1996; Lourens et al., 2004; Backman et al., 2012). Interestingly, both *H. ampliaperta* and *S. heteromorphus* presented a similar pattern displaying low abundances long before their final disappearance. Indeed *H. ampliaperta* shows discontinuous and scattered distribution in its upper range (see Backman et al., 2012). In addition, *S. heteromorphus* distribution displays an interval of prominently reduced abundance or absence (paracme interval mostly exhibited in between 14.59 and17.32 m of the KHS), well-documented in other Mediterranean successions (Di Stefano et al., 2008, 2011; Fornaciari et al., 1996; Iaccarino et al., 2011; Triantaphyllou, 2010); base and top of this paracme are dated at 15.949 Ma and 15.527 Ma respectively (Di Stefano et al., 2008). The KHS data suggest that

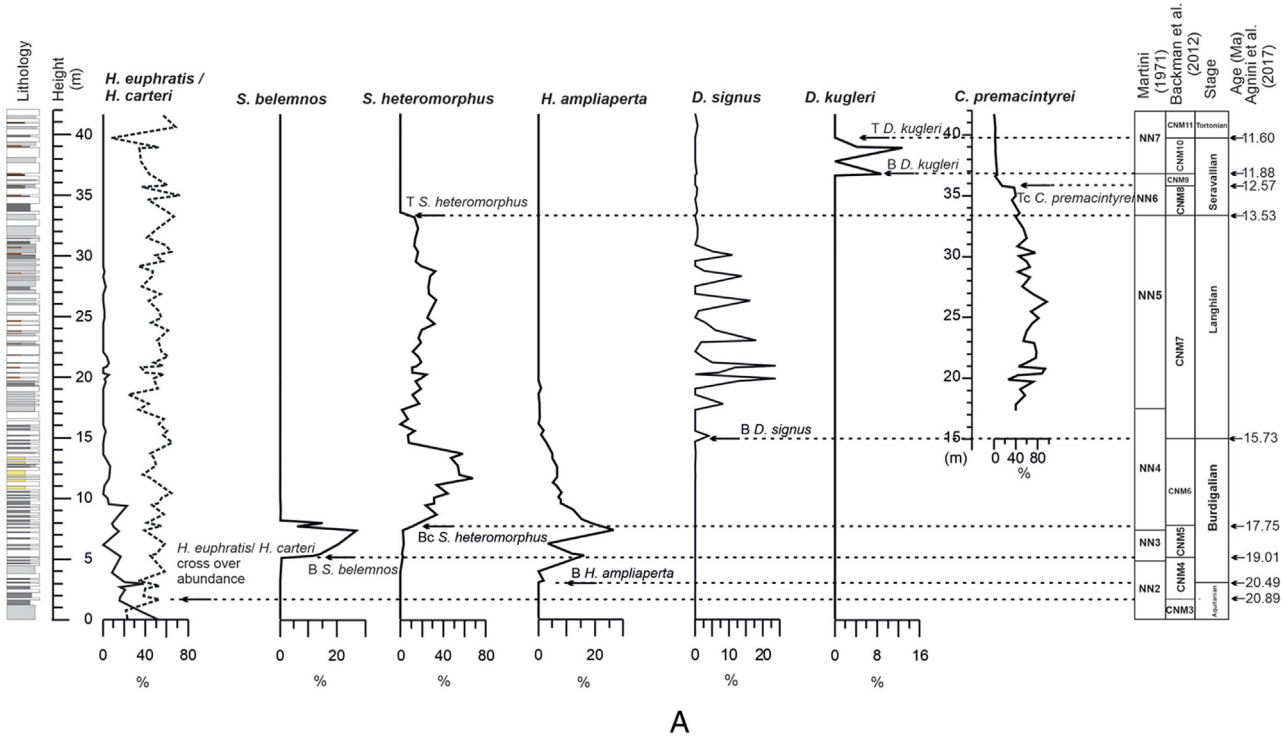

Fig. 3. (a) Calcareous Nannofossil biohorizons (CN; Agnini et al., 2017) detected at the KHS record and biostratigraphic assignment, following Backman et al. (2012) and Martini (1971) nannofossil zonal schemes; ages are after Agnini et al. (2017). Abbreviations as follows: B-base, Bc-base common, T-top, Tc-top common, FO-First Occurrence, **(b)** Age versus height plot produced for the 17–42 m KHS interval. **c.** Spectral analysis of the lithological variations; signal amplitude vs. frequency (in kyr^{-1}) and (embedded figure) signal amplitude vs. period (in kyr) with focus on the 15-30 kyr period. The red horizontal line indicates the statistical significance at a = 0.01. (For interpretation of the references to colour in this figure legend, the reader is referred to the web version of this article).

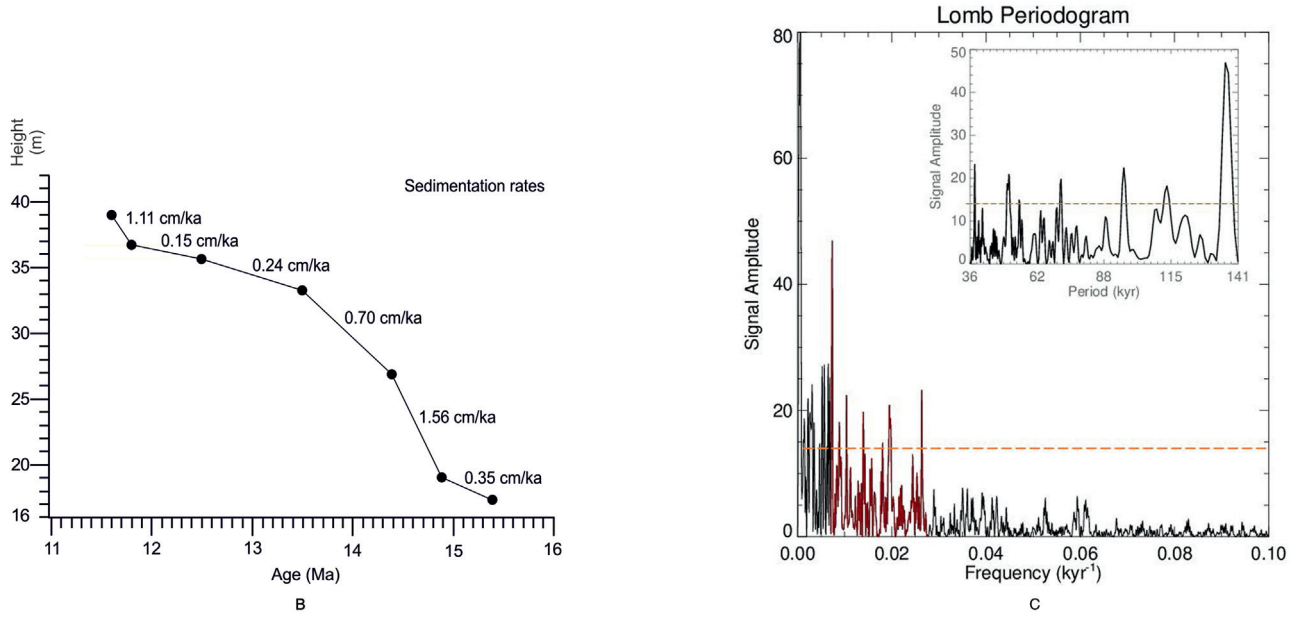

Fig. 3. (*continued*).

S. heteromorphus has never fully recovered to high values after entering the paracme interval, following a rather uniform pattern with low abundances up to its disappearance level at 33.22 m (13.53 Ma). The top common (Tc) of *C. premacintyrei* at 35.65 m, corresponds to the CNM8/CNM9 boundary within NN9 biozone (12.57 Ma; Backman et al., 2012). Total range of *D. kugleri* is observed between 36.70 m and 38.92 m with values from 4.2 to 12.7% possibly corresponding to both the Bc and Tc *D. kugleri* and dated at 11.88 Ma and 11.60 Ma respectively. Planktonic foraminifer *Orbulina universa* appeared at 22.89 m providing an age of 14.36 Ma (Abdul Aziz et al., 2008; Lirer et al., 2019) for the specific level of the section.

From a biostratigraphical point of view the KHS sequence spans Zone CNM3 to Zone CNM11 (Backman et al., 2012; Agnini et al., 2017) or Zone NN2 to Zone NN7 (Martini, 1971), which correspond to ~20.89–11.6 Ma time interval (late Aquitanian to early Tortonian). Based on the resolved CN biohorizons (Table 1), the age depth plot has been constructed for the KHS (Fig. 3b). The estimated sedimentation rates within the ~15–33 m and ~37–39 m intervals, appear higher than the corresponding rates in between ~33–37 m and the part of the section corresponding to lowest 15 m, mostly comprising marly chalks and chalky marls (see Figs. 2, 3b). Apparently, hiatuses cannot be excluded, especially at 33 m, where either slow sedimentation or even a gap might be recorded. However, the succession of the detected CN biohorizons in the KHS record, enables us to consider such hiatuses too short to be clearly detected, therefore a continuous age model has been constructed by linear interpolation between the fixed tie points.

The spectral analysis indicates that the numerical string of the lithology exhibited several statistically significant periodic signals (at a = 0.001). Prominent frequency peaks, statistically significant above the 99% confidence level, are present, corresponding to ~1700 kyr, ~136 kyr, ~96 kyr, ~51 kyr and ~38 kyr (Fig. 3c). The period of 1700 kyr could be attributed to very long eccentricity terms (Boulila et al., 2014), while the other peaks are consistent with orbital eccentricity and with obliquity terms.

4.3.2. Calcareous Nannofossil assemblages

The total assemblage of the upper KHS sequence (19.74–38.92 m height) was dominated by species belonging to the Noelaerhabdaceae family (mostly *Reticulofenestra* spp. spp. <6 μm, *Dictyococcites* spp., *Cyclicargolithus* spp.), followed by the cool-water mesotrophic taxa *Coccolithus* spp.-*Calcidiscus* spp. The rest of the assemblage consisted of *Discoaster* spp. (*D. deflandrei, D. variabilis, D. exilis, D. signus* and *D. kugleri*), *Sphenolithus* spp. (mostly *Sphenolithus moriformis, S. heteromorphus, S. compactus*; *S. abies* is present with low abundance, up to 11%, above 38 m height), *Helicosphaera* spp. (*Helicosphaera carteri, H. intermedia, H. mediterranea, H. waltrans, H. walbersdorfensis, H. orientalis* and *H. stalis*, and less common species such as *H. ampliaperta* and *H. obliqua*) and the less frequent *Umbilicosphaera* (primarily *U. jafari* and *U. rotula*), *Rhabdosphaera* spp., *Syracosphaera* spp. and reworked specimens (see Appendix 1). Observations under LM and SEM revealed variations, from poor to excellent, in the preservation of calcareous nannofossils

Table 1
Calcareous Nannofossil and Planktonic Foraminifera biohorizons used in the present study.

Biohorizon	Height (m)	Age (Ma)	Reference
T *D. kugleri*	38.92	11.6	Agnini et al. (2017)
B *D. kugleri*	36.70	11.88	Agnini et al. (2017)
Tc *C. premacintyrei*	35.65	12.57	Agnini et al. (2017)
T *S. heteromorphus*	33.22	13.53	Agnini et al. (2017)
FO *O. universa* *	22.89	14.36	Lirer et al. (2019)
T paracme *S. heteromorphus**	17.32	15.527	Di Stefano et al. (2008)
B *D. signus*	15.21	15.73	Agnini et al. (2017)
B paracme *S. heteromorphus**	14.59	15.949	Di Stefano et al. (2008)
Bc *S. heteromorphus*	7.71	17.75	Agnini et al. (2017)
B *S. belemnos*	5.28	19.01	Agnini et al. (2017)
B *H. ampliaperta*	3.20	20.49	Agnini et al. (2017)
H. euphratis/ H. carteri cross over abundance	1.70	20.89	Agnini et al. (2017)

depending on the lithology. The preservation was generally good in marl and siltstone, while poorly preserved nannofossil assemblages were observed in chalky marl and chalk. Abundance patterns of the representative taxa are plotted in Fig. 4a as counts in a total of 500 nannofossil specimens.

Taxa of the Noelaerhabdaceae family consisting of *Reticulofenestra* spp. (~25% on average), *Cyclicargolithus* spp. (average ~23%), and *Dictyococcites* spp., (average ~15%), reached up to 85% in chalk, showing minima within the thin TOC rich-laminated siltstone layers (layers 1–17; Fig. 4a). *Umbilicosphaera jafari, Coccolithus* spp., *Calcidiscus* spp. displayed similar patterns reaching ~18% and ~33% respectively, with the latter exhibiting sharp increase in the following intervals: 22.3–24.2, 25.8–29.4, 31.9–34.9 and 37.4–39.4 m (Fig. 4a). Opposite patterns have been observed for the *Discoaster* spp. (max. ~11%), *Sphenolithus* spp. (max. ~25%), *Helicosphaera* spp. (max. ~21%), and *Rhabdosphaera* spp. (max. ~10%) (Fig. 4a). *Syracosphaera* spp., *Umbilicosphaera* and reworked specimens, along with *Rhabdosphaera* spp., exhibited an increase from 33 m and upwards (layers 14–17; Fig. 4a).

4.4. Pollen and palynomorphs

Palynomorphs were preserved in all siltstone layers, while samples from chalk and chalky marl were either devoid in pollen and palynomorphs, especially in the lower part of the studied interval, or contained very low amounts. Terrestrial pollen and spore concentrations were low (average *rotula* 2500 grains/g); however, it was enhanced in the lower part of the section (17–42 m; Fig. 4b), reaching a maximum of 25,000 grains/g. Pollen assemblages were characterized by high abundances of Arboreal Pollen (AP) especially *Pinus* and Taxodiaceae/Cupressaceae. *Cedrus, Quercus, Ulmus/Zelkova, Tsuga* and *Acacia* comprised additional AP records. The concentration of fungal remains (mostly Type 207, a mycorrhizal fungus; Van Geel et al., 1989) was significantly higher compared to pollen and spores, showing average values of 5500 grains/g increasing in the upper part of the studied KHS interval (Fig. 4b). Finally, microscopic charcoal frequencies followed a similar to Type 207 distributional trend (max. 4600 particles/g).

4.5. Oxygen and carbon isotope record

The oxygen isotope composition of the planktonic foraminifera *O. universa* ($\delta^{18}O$) ranged from -0.95 to 0.82 ‰ VPDB, across the investigated interval (Figs. 4a, 5). The lowest values of the $\delta^{18}O$ were recorded at 22.2 m, 34.6 m, 36.7 m and 39 m of the KHS (layers 5, 16, 17), while relatively high values have been observed at 28.6 m and 33.9 m. A general trend towards heavier values was observed between 24 m and 34 m, where the $\delta^{18}O$ values gradually increased from −0.58 up to 0.82 ‰.

The carbon isotope composition of *O. universa* ($\delta^{13}C$) varied between 1.09 and 2.26 ‰ VPDB (Figs. 4a, 5). The $\delta^{13}C$ maximum values were recorded around 23.8, 33.2, 35.7 and 38.9 m, while minima were observed around 23, 26.3, 34.2 and 36.2 m. A two-step increase (ca. 0.9 ‰) was observed between 28 and 33 m.

5. Discussion

5.1. Paleoceanographic reconstruction in-between 15.2–11.6 Ma

Within the upper part of the KHS sequence the abundance peaks of *Rhabdosphaera* spp., *Syracosphaera* spp., *Helicosphaera* spp. were observed mostly within the thin laminated TOC-enriched siltstone intercalations (layers 1–17; Fig. 4b). The upper photic zone taxa Rhabdosphaeraceae and *Syracosphaera* spp. prefer warm and oligotrophic waters in the modern ocean (Ziveri et al., 2004; Triantaphyllou et al., 2004; Dimiza et al., 2008; Malinverno et al., 2009). *Rhabdosphaera* spp. and *Syracosphaera* spp. also displayed higher abundance in oligotrophic tropical settings during Pliocene (Gibbs et al., 2004; Bolton, 2010). The *Helicosphaera* species (max. ~20%, mostly *H. carteri*; Fig. 4b) are reported to prefer shallow, eutrophic, or hyposaline environments (Perch-Nielsen, 1985; Wade and Bown, 2006; Dimiza et al., 2014), and higher

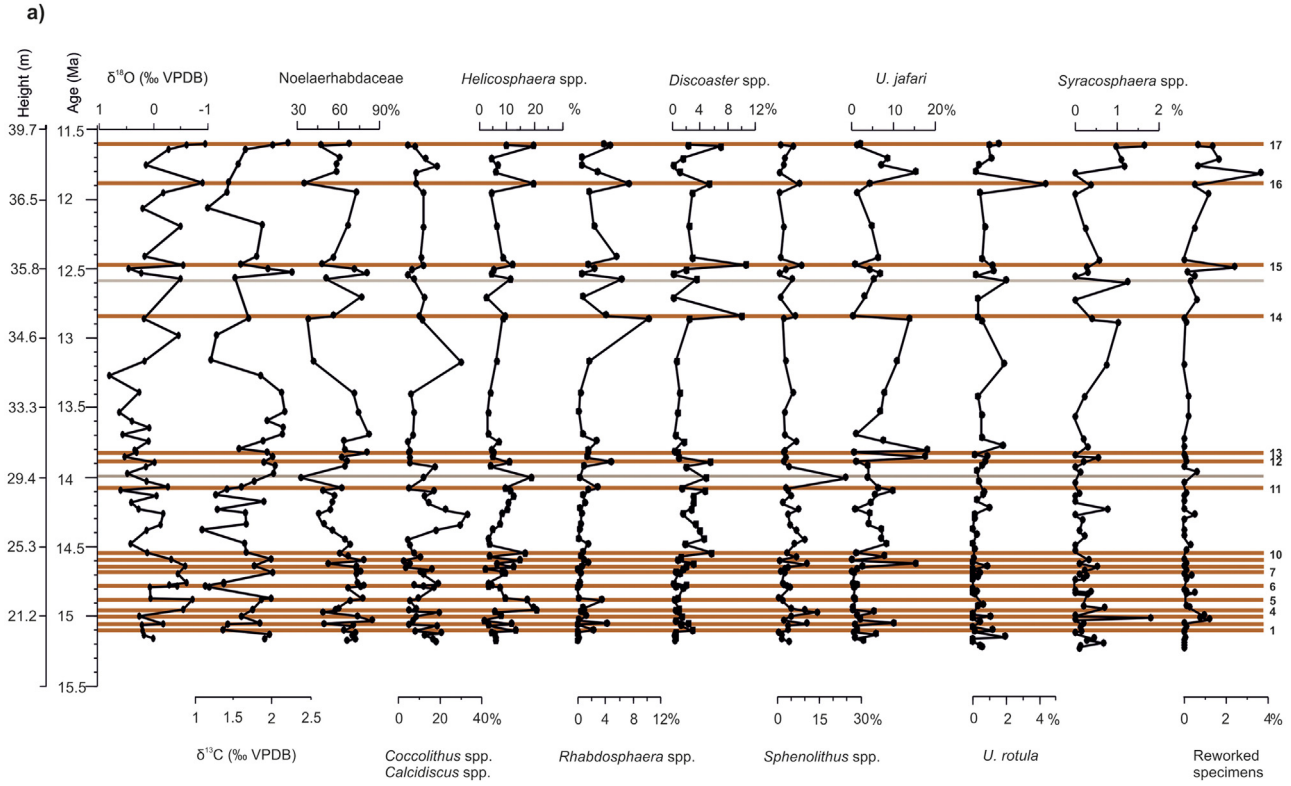

Fig. 4. (a) Dominant calcareous nannofossil species relative abundances, counted in 500 nannofossil specimens. **(b)** Pollen and palynomorph absolute abundances. Siltstone laminated layers are highlighted in brown bands.

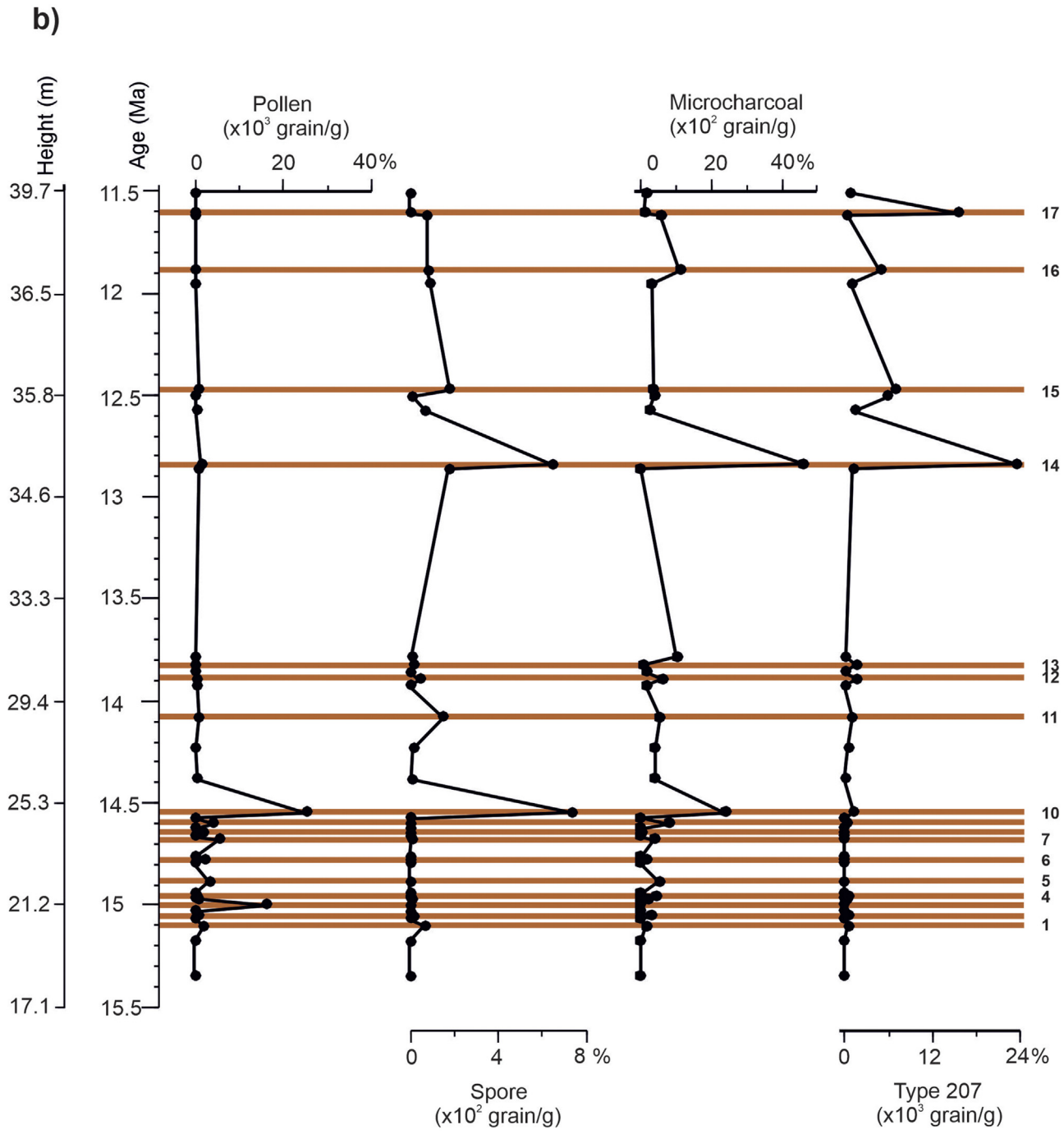

Fig. 4. (*continued*).

productivity regions (Ziveri et al., 2004). They have been associated with higher fresh water input during periods of sapropel deposition in the eastern Mediterranean within Pleistocene and Holocene (Colmenero-Hidalgo et al., 2004; Triantaphyllou et al., 2009, 2010) but also in the Pliocene (Athanasiou et al., 2015, 2017).

Simultaneous peaks within the TOC-enriched layers were observed in the abundance patterns of *Sphenolithus* spp. and *Discoaster* spp. (particularly in layers 10–17; Fig. 4a). Discoasters have been found to thrive in oligotrophic tropical deep waters during Miocene and Pliocene (Athanasiou et al., 2015; Flores et al., 1992; Gibbs et al., 2004; Vázquez et al., 2000), and are considered increasing their abundance with deep pycnocline as lower photic zone inhabitants (Flores et al., 2005). Sphenoliths have been reported as sharing similar ecological preferences as the discoasters in warm, oligotrophic environments (e.g. Haq, 1980; Lohmann and Carlson, 1981; Perch-Nielsen, 1985; Aubry, 1992).

Overall, the nannofossil distribution in the upper part of KHS (~20–40 m) designate warm and oligotrophic surface waters with indication of lowering of salinity during the deposition of the TOC-enriched layers (especially 10–17 at the ~29–40 m part of the section; Fig. 4a). In particular, *Discoaster* spp. patterns mostly in layers 12, 14–17, could also support a productive lower photic zone associated with water column stratification, as already suggested by different authors (Flores et al., 2005; Athanasiou et al., 2015, 2017). The decreased $\delta^{18}O$ values observed in the same layers (Fig. 4a) sustain the prevalence of warm surface water masses and enhanced freshwater input into the basin (e.g., Turco et al., 2001; Mourik et al., 2011; Triantaphyllou et al., 2016), with

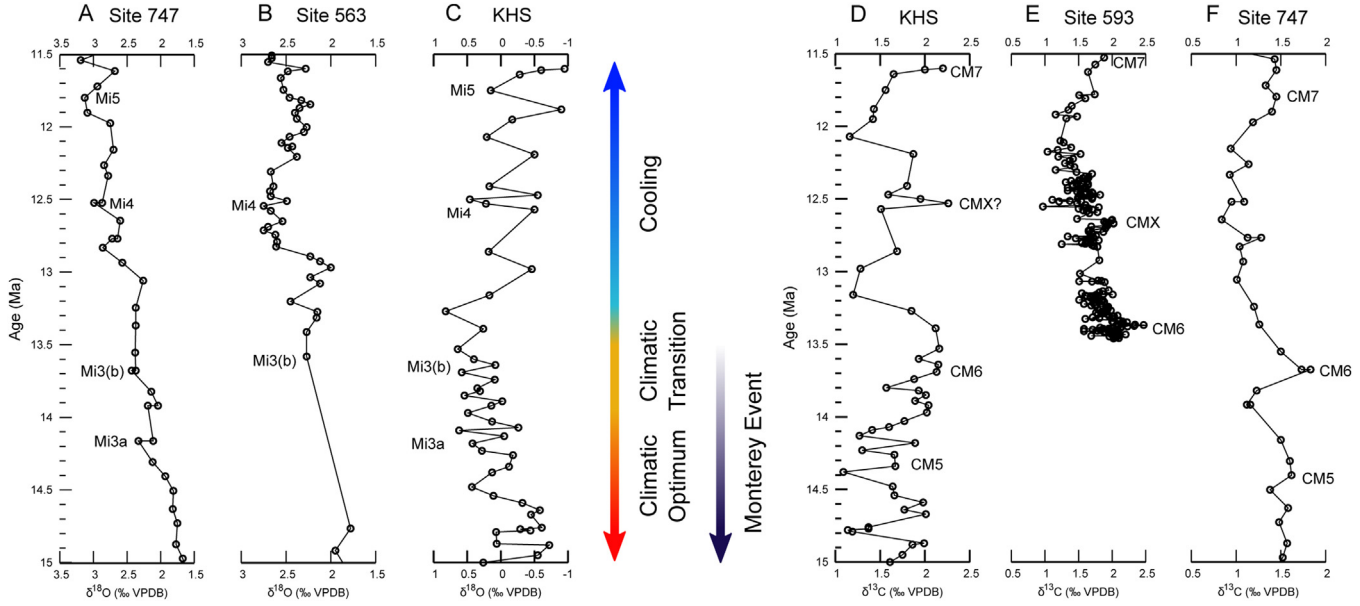

Fig. 5. Paleoclimatic implications for the Kottafi Hill sequence, based on the oxygen and carbon isotope composition of the planktonic foraminifer *Orbulina universa*, and comparison with the global isotopic records. $\delta^{18}O$ profiles: A. Site 747: data from Zachos et al. (2001); Mi-events after Berrgren et al. (1995) from Zachos et al. (2001), B. Site 563: data from Zachos et al. (2001); Mi-events after Miller et al. (1991), C. KHS: Kottafi Hill Section. $\delta^{13}C$ profiles: D. KHS: Kottafi Hill Section, E. Site 593: data from Cooke et al. (2008); CM-events after Cooke et al. (2008), F. Site 747: data from Zachos et al. (2001); Mi-events after Woodruff and Savin (1991).

the latter interpretation further supported by the accompanied elevated abundances of *Helicosphaera* spp. Remarkably, there are at least two more levels in the studied KHS record (grey lines in between layers 11–12 and 14–15 respectively; Fig. 4a) that exhibit increases in *Sphenolithus* spp. (max. ~25% at 29.4 m) accompanied by small positive shifts in the abundance of the nannofossil taxa except of Noelaerhabdaceae and *Coccolithus* spp.-*Calcidiscus* spp. Most probably these layers represent likewise rather warm and oligotrophic intervals, yet too short to be imprinted in the lithological record.

Considering the results derived from the palynological analysis, the well-preserved pollen and their increased abundance within the siltstone laminae of the 20–25 m interval of KHS suggest densely-vegetated borderlands till ~14.5 Ma (Fig. 4b). Moreover, the distribution trend of the land-derived palynomorphs, such as spores and microcharcoal, provides evidence for relatively low terrigenous inputs within the siltstone layers until ~14.5 Ma (17.1–25.3 m; Fig. 4b). In contrast, the palynomorph signal above the 35 m level of KHS (~13.0–11.6 Ma), implies rather open landscapes, thus easily to be eroded during time intervals of high humidity. The peaks of the palynomorph Type 207 in layers 14–17 (see Fig. 4b) can support the aforementioned interpretation. Type 207 is a mycorrhizal fungus occurring in the roots of a variety of host plants and is a good indicator of terrestrial soil erosion when found in marine sedimentary records (Anderson et al., 1984; Triantaphyllou et al., 2009; van Geel et al., 1989). The simultaneous increase of reworked nannofossil specimens, especially in layer 15 (Fig. 4a) further justifies the land erosion processes.

Hence, marine and terrestrial evidence during 15.5–11.6 Ma, point to warm and oligotrophic conditions combined with water column stratification over time intervals of a wetter climate in the eastern Mediterranean Basin, associated with the deposition of the TOC-enriched layers 1–17 in the KHS record. Our micropaleontological, palynological and isotope evidence indicate that such conditions were more intense within layers 14–17, in between ~13.0–11.6 Ma (Fig. 4a), opposite to milder events associated with the formation of layers 1–13. This is in accordance to Mourik et al. (2011) who suggested dry-wet climate oscillations after 13.1 Ma, with seasonally enhanced influx of fresh water and/or changes in the evaporation rates. Analogous contemporaneous changes in the hydrology and nutricline dynamics of eastern Mediterranean areas have triggered the deposition of Quaternary and Holocene sapropels (e.g., Bouloubassi et al., 1999; Rohling et al., 2002, 2015; Triantaphyllou et al., 2009, 2010; Triantaphyllou, 2014; Grelaud et al., 2012) and Pliocene sapropelic layers (e.g., Lourens et al., 1992; Athanasiou et al., 2015, 2017). As firstly proposed by Rossignol-Strick (1985), sapropel formation in the eastern Mediterranean has been controlled by the orbital precession causing intensification of the North African monsoon and subsequent flooding, mainly through the Nile River discharges (see Rohling, 1994; Rohling et al., 2015). The shoaling of the pycnocline/nutricline and the presence of Levantine Intermediate Water (LIW) at shallow water depths have favoured the injection of nutrients, the enhancement of marine productivity in the lower photic zone (e.g., Castradori, 1993, 1998; Grelaud et al., 2012) and consequent preservation of the organic matter at the sea bottom resulted in the deposition of sapropelic layers (e.g., Rohling, 1994; Rohling et al., 2015; Emeis et al., 2000; Triantaphyllou et al., 2009). Sapropel formations of a late Miocene age are mainly known from outcrops in Italy and Malta of the central Mediterranean region (e.g., Hilgen et al., 2003; Mourik et al., 2010), and from deposits in the Crete Island of the eastern Mediterranean region (Nijenhuis et al., 1996).

Thus, we assume that the TOC-rich siltstone laminae of the KHS record represent the Miocene precursors of the sapropels/sapropelic layers developed in eastern Mediterranean during the Plio-Pleistocene. Single evidence of Langhian sapropelic layer has been reported so far on land sequence from Cyprus dated at 15.4 Ma (Taylforth et al., 2014). Interestingly, the spectral analysis in the KHS sedimentary record, although consistent with orbital eccentricity and obliquity terms (Fig. 3c), did not reveal the precession signal influence, related to the sapropel formation in the eastern Mediterranean (e.g., Lourens et al., 1992). Its absence could be attributed to the relatively low temporal resolution of the investigated lithological record due to loose sampling spacing that resulted in the scattered occurrence of the sapropel-like layers of KHS, eliminating the precession imprint (e.g., Lu et al., 2004).

The thin KHS siltstones are interbedded with chalk, chalky marl and marly chalk facies that are characterized by the dominance of the Noelaerhabdaceae family (mostly *Reticulofenestra* spp., *Dictyococcites* spp., *Cyclicargolithus* spp.), followed by the cool-water mesotrophic taxa *Coccolithus* spp.-*Calcidiscus* spp. (Fig. 4a). *Reticulofenestra* spp. are

considered as opportunistic taxa of the upper photic zone, indicating high nutrient conditions established under intense mixing of the surface waters (Gartner, 1988; Flores et al., 2005). Ecological affinities of *Dictyococcites* spp. can link the high abundances of these taxa to cold-water masses (e.g., Kameo and Sato, 2000); implying the input of cooler, nutrient-rich waters in the broader study area. In accordance, *Coccolithus* spp. has affinities with upwelling (Baumann et al., 2000), relatively increased water column turbulence and/or nutrient availability (Negri et al., 2003). The increased presence of both Noelaerhabdaceae *Coccolithus* spp.-*Calcidiscus* spp. accompanied by higher $\delta^{18}O$ values, indicate cooler climatic conditions during the deposition of the chalk, chalky marl and marly chalk facies (Fig. 4a). Associated positive peaks of *U. jafari* may indicate salinity increase similarly to late Messinian (Flores et al., 2005; Wade and Bown, 2006) or Pliocene evidence (Athanasiou et al., 2015, 2017). A slight increase of both $\delta^{18}O$ values and the cool-water mesotrophic nannofossil taxa observed at 37.75 m (11.75 Ma), can be related to a cooling episode. Similar pattern of increased values of the $\delta^{18}O$, coinciding within the short biostratigraphic range of *D. kugleri* (CNM10 biozone), has been also reported in the Mediterranean by Turco et al. (2001).

5.2. Miocene paleoclimatic implications in the eastern Mediterranean

Dynamically changing Miocene climate is characterized by several global events (Fig. 5). The MCO turned into the mMCT to finally develop into the cooling period linked with the expansion of the East Antarctic Ice Sheet at around 13.8 Ma (Miller et al., 1991; Flower and Kennett, 1994; Zachos et al., 2001). A gradual accumulation of the Antarctic ice sheet led to the major deep-water circulation changes and glacial events which are globally observed in the $\delta^{18}O$ records (Miocene oxygen isotope events, Mi1-Mi7 events; e.g., Miller et al., 1991; Wright and Miller, 1992; Miller et al., 1998; Cooke et al., 2008; John et al., 2011). The Mi-events coincide with carbon maxima (CM1-CM7; Woodruff and Savin, 1985, 1991), which are evidences of accumulation of organic carbon-rich sediments during the Miocene and recorded as increased $\delta^{13}C$ values. The CM1-CM6 events are associated with the Monterey Excursion, which is observed as a long-lasting $\delta^{13}C$ positive shift (ca.17−13.5 Ma; Vincent and Berger, 1985; Woodruff and Savin, 1985).

Oxygen isotope composition of marine calcite fossils may reflect changes in paleotemperature and global ice volume (Faure, 1977; Zachos et al., 1993; Billups and Spero, 1996) with the lower values of $\delta^{18}O$ observed during warm interglacial periods and higher values during cool glacial periods (Faure, 1977). In addition, lower $\delta^{18}O$ values can be attributed to fresh water supply and decrease of salinity (Paul et al., 1999). In turn, variations in carbon isotope composition of marine carbonates are used as a proxy of marine productivity (Faure, 1977; Zachos et al., 1993).

Events Mi3a-Mi5 and CM5-CM7 are recognised in the planktonic foraminifera $\delta^{18}O$ records from the KHS (Fig. 5) using the criteria of Miller et al. (1991) and further revised ages (Woodruff and Savin, 1991; Wright and Miller, 1992; Berggren et al., 1995; Zachos et al., 2001, 2008). The slight age discrepancies of recorded events may be the result of the limited datings available in the middle Miocene interval of the KHS. Discrepancies may also arise because the original designations are based on the benthic records which are more likely to record global signals. A positive shift of the $\delta^{18}O$ values observed between ca. 14.7 and 13.3 Ma along the KHS, reflects stepwise cooling during the mMCT: the Mi3a event, which is considered as a minor phase and the following Mi3b event considered as a major one (e.g., Shevenell et al., 2004; Tian et al., 2009, 2013; Fig. 5). In contrast to some previously published Miocene $\delta^{18}O$ records (e.g., Wright and Miller, 1992; Cooke et al., 2008; Zachos et al., 2008), the observed $\delta^{18}O$ values of the planktonic foraminifera from the KHS decrease gradually after Mi3b event. The $\delta^{18}O$ negative trend was previously recorded between 13 and 11 Ma in Malta and was interpreted as a possible effect of the isolation of the Mediterranean Sea that led to increased influx of fresh water and changes in salinity and/or sea water temperature (Jacobs et al., 1996). The Mi3b event coincides with the CM6 which marks the end of the Monterey Excursion. The Mi4 event coincides with a carbon maximum (CMX), which has been previously described from the deep-water record of the Hole 593 (Cooke et al., 2008). According to Woodruff and Savin (1991), the Mi5 event corresponds to CM7, however in the $\delta^{18}O$ record of KHS there is a slight lag between Mi5 event and the observed shift of the $\delta^{13}C$values.

Identification of the Mi-events and CM in the oxygen and carbon isotope records of the KHS indicates documentation of the global climate changes in this section. However, since estimations of the Mi- and CM-events in the KHS described above rely on purely biostratigraphically dated sediments, astronomical tuning of the KHS aiming to a more accurate age-control, is essential to confirm the presence of these major cooling steps in the study area. A higher-resolution and well-tuned isotopic record should provide a better understanding of the middle Miocene cooling events and support an interpretation of global and regional causes of its variations.

6. Conclusions

The main findings of this study are summarized below:

- The Kottafi Hill section is assigned to nannofossil biozones CNM3–CNM11 or NN2–NN7, which correspond to the 20.89–11.6 Ma time interval.
- The TOC-rich siltstone laminae, intercalated in the KHS carbonate record, have been deposited between 15.5 and 11.6 Ma, equivalent to CNM7–CNM11 (NN5–NN7) biozones. The environmental conditions under which these laminae have been formed, are associated with warm and oligotrophic waters, productive lower photic zone with strong water column stratification, enhanced freshwater influx and depositional cyclicity, suggesting them as the precursors of the sapropels/sapropelic layers developed in the eastern Mediterranean. In contrast, the chalk, chalky marl and marly chalk facies of KHS have been deposited under nutrient-rich waters and cooler climatic intervals.
- The Mi3–Mi5 events and CM5–CM7 episodes of the middle Miocene, are identified in the planktonic foraminifera oxygen and carbon isotope records of KHS indicating an evident impact of the middle Miocene global climate changes on the carbonate deposition in this region.

Declaration of interests

The authors declare that they have no known competing financial interests or personal relationships that could have appeared to influence the work reported in this paper.

Acknowledgments

Funding was provided by the European Research Project MarinERA/MedEcos and Research Project KA 70/4/11078 of the National and Kapodistrian University of Athens. Thoughtful discussions with Emma Sheldon are greatly appreciated. The authors are grateful to the Cyprus Geological Survey for the support provided during the field work at the Kottafi Hill section. Thanks are due to Fotini Efthymiou for technical assistance during the sample processing.

Appendix A. Supplementary data

Supplementary material related to this article can be found, in the online version, at doi:https://doi.org/10.1016/j.revmic.2020.100480.

References

Abdul Aziz, H., Di Stefano, A., Foresi, L.M., Hilgen, F.J., Iaccarino, S.M., Kuiper, K.F., Lirer, F., Salvatorini, G., Turco, E., 2008. Integrated stratigraphy and 40Ar/39Ar chronology of early Middle Miocene sediments from DSDP Leg 42A, Site 372 (Western Mediterranean). Palaeogeogr. Palaeoclimatol. Palaeoecol. 257, 123–138.

Abels, H.A., Hilgen, F.J., Krijgsman, W., Kruk, R.W., Raffi, I., Turco, E., Zachariasse, W.J., 2005. Long-period orbital control on middle Miocene global cooling: integrated stratigraphy and astronomical tuning of the Blue Clay Formation on Malta. Paleoceanography 20 https://doi.org/10.1029/2004PA001129.

Agnini, C., Monechi, S., Raffi, I., 2017. Calcareous nannofossil biostratigraphy: historical background and application in Cenozoic chronostratigraphy. Lethaia 50, 447–463.

Anderson, R.S., Homola, R.L., Davis, R.B., Jacobson Jr., G.L., 1984. Fossil remains of the mycorrhizal fungal *Glomus fasciculatum* complex in postglacial lake sediments from Maine. Can. J. Bot. 62, 2325–2328.

Athanasiou, M., Triantaphyllou, M., Dimiza, M., Gogou, A., Bouloubassi, I., Tsiolakis, E., Theodorou, G., 2013. Early-Middle Miocene from Kotaphi Hill section (Nicosia, Cyprus): biostratigraphy and paleoceanographic implications. Bulletin of the Geological Society of Greece, Proceedings of the 13th International Congress, XLVII/1 62–71.

Athanasiou, M., Triantaphyllou, M.V., Dimiza, M.D., Gogou, A., Theodorou, G., 2015. Zanclean/Piacenzian transition on Cyprus (SE Mediterranean): calcareous nannofossil evidence of sapropel formation. Geo-Marine Lett. 35, 367–385.

Athanasiou, M., Bouloubasi, I., Gogou, A., Klein, V., Dimiza, M.D., Parinos, C., Skampa, E., Triantaphyllou, M.V., 2017. Sea surface temperatures and environmental conditions during the "warm Pliocene" interval (~4.1–3.2 Ma) in the Eastern Mediterranean (Cyprus). Glob. Planet. Change 150, 46–57.

Aubry, M.-P., 1992. Late Paleogene nannoplankton evolution: a tale of climatic deterioration. In: Prothero, D.R., Berggren, W.A. (Eds.), Eocene-Oligocene Climatic and Biotic Evolution. Princeton Univ. Press, Princeton, N.J, pp. 272–309.

Auer, G., Piller, W.E., Reuter, M., Harzhauser, M., 2015. Correlating carbon and oxygen isotope events in early to middle Miocene shallow marine carbonates in the Mediterranean region using orbitally tuned chemostratigraphy and lithostratigraphy. Paleoceanography https://doi.org/10.1002/2014PA002716.

Backman, J., Raffi, I., Rio, D., Fornaciari, E., Pälike, H., 2012. Biozonation and biochronology of Miocene through Pleistocene calcareous nannofossils from low and middle latitudes. Newsl. Stratigr. 45, 221–244.

Baumann, K.H., Andruleit, H., Samtleben, H., 2000. Coccolithophores in the Nordic Seas: comparison of living communities with surface sediment assemblages. Deep Sea Res. Part II Top. Stud. Oceanogr. 47, 1743–1772.

Berggren, W.A., Kent, D.V., Swisher, C.C., Aubry, M.-P., 1995. A revised Cenozoic geochronology and chronostratigraphy. In: Berggren, W.A., Kent, D.V., Aubry, M.-P., Hardenbol, J. (Eds.), Geochronology, Time Scales and Global Stratigraphic Correlation: A Unified Temporal Framework for an Historical Geology, 54. Special publication — Society of Economic Paleontologists and Mineralogists, pp. 29–212.

Béthoux, J.P., 1993. Mediterranean sapropel formation, dynamic and climatic viewpoints. Oceanol. Acta 16, 127–133.

Billups, K., Spero, H., 1996. Reconstructing the stable isotope geochemistry of the equatorial Atlantic during the last 150,000 years: results from individual foraminifera. Paleoceanography 11, 217–238.

Bolton, C.T., 2010. Orbital and Suborbital Climate Variability during the Pliocene Intensification of Northern Hemisphere Glaciation. PhD thesis. University of Southampton 250 pp.

BouDagher-Fadel, M., Lord, A., 2006. Illusory stratigraphy decoded by Oligocene-Miocene autochthonous and allochthonous foraminifera in the Terra Member, Pakhna Formation (Cyprus). Stratigraphy 3, 217–226.

Boulila, S., Galbrun, B., Huret, E., Hinnov, L.A., Rouget, I., Gardin, S., Huang, C., Bartolini, A., 2014. Astronomical calibration of the Toarcian Stage: implications for sequence stratigraphy and duration of the early Toarcian OAE. Earth Planet. Sci. Lett. 386, 98–111.

Bouloubassi, I., Rullkötter, J., Meyers, P.A., 1999. Origin and transformation of organic matter in Pliocene–Pleistocene Mediterranean sapropels: organic geochemical evidence reviewed. Mar. Geol. 153, 177–197.

Bown, P.R., Young, J.R., 1998. Techniques. In: Bown, P.R. (Ed.), Calcareous Nannofossil Biostratigraphy. Chapman and Hall, Kluwer Academic, pp. 16–28.

Brandano, M., 2017. Unravelling the origin of a Paleogene unconformity in the Latium-Abruzzi carbonate succession: a shaved platform. Palaeogeogr. Palaeoclimatol. Palaeoecol. 485, 687–696.

Brandano, M., Cornacchia, I., Raffi, I., Tomassett, L., Agostini, S., 2017. The Monterey Event within the Central Mediterranean area: the shallow-water record. Sedimentology 64, 286–310.

Burke, K.D., Williams, J.W., Chandlerc, M.A., Haywoode, A.M., Luntf, D.J., Otto-Bliesnerg, B.L., 2018. Pliocene and Eocene provide best analogs for near future climates. PNAS 115, 13288–13293.

Casford, J.S.L., Rohling, E.J., Abu-Zied, R.H., Fontanier, C., Jorissen, F.J., Leng, M., Schmiedl, G., Thomson, J., 2003. A dynamic concept for eastern Mediterranean circulation and oxygenation during sapropel formation. Palaeogeogr. Palaeoclimatol. Palaeoecol. 190, 103–119.

Castradori, D., 1993. Calcareous nannofossil and the origin of Eastern Mediterranean sapropels. Paleoceanography 8, 459–471.

Castradori, D., 1998. Calcareous nannofossils in the basal Zanclean of the eastern Mediterranean Sea: remarks on paleoceanography and sapropel formation. Proc. Ocean Drill. Prog. Sci. Results 160, 113–123.

Colmenero-Hidalgo, E., Flores, J.A., Sierro, F.J., Bárcena, M.Á., Löwemark, L., Schönfeld, J., Grimalt, J.O., 2004. Ocean surface water response to short-term climate changes revealed by coccolithophores from the Gulf of Cadiz (NE Atlantic) and Alboran Sea (W Mediterranean). Palaeogeogr. Palaeoclimatol. Palaeoecol. 205, 317–336.

Cooke, P.J., Nelson, C.S., Crundwell, M.P., 2008. Miocene isotope zones, paleotemperatures, and carbon maxima events at intermediate water-depth, site 593, Southwest Pacific. New Zealand J. Geol. Geophys. 51, 1–22.

Davies, Q.J., 2001. Climatic and Tectonic Controls on Deep Water Sedimentary Cyclicity; Evidence from the Miocene to Pleistocene of Cyprus. Ph.D. Thesis. The Open University, Milton Keynes, England.

De Lange, G.J., Thomson, J., Reitz, A., Slomp, C.P., Principato, M.S., Erba, E., Corselli, C., 2008. Synchronous basin-wide formation and redox-controlled preservation of a Mediterranean sapropel. Nat. Geosci. 1, 606–610.

Di Stefano, A., Foresi, L.M., Lirer, F., Iaccarino, S.M., Turco, E., Amore, F.O., Mazzei, R., Morabito, S., Salvatorini, G., Aziz, H.A., 2008. Calcareous plankton high resolution bio-magnetostratigraphy for the Langhian of the Mediterranean area. Rivista Italiana di Paleontologia e Stratigrafia 114, 51–76.

Di Stefano, A., Verducci, M., Cascella, A., Iaccarino, S.M., 2011. Calcareous plankton events at the Early/MiddleMiocene transition of DSDP Hole 608: comparison with Mediterranean successions for the definition of the Langhian GSSP. Stratigraphy 8, 145–161.

Di Stefano, A., Foresi, L.M., Incarbona, A., Sproveri, M., Vallefuoco, M., Iorio, M., Pelosi, N., Di Stefano, E., Sangiorgi, P., Budillon, F., 2015. Mediterranean Coccolithophore Ecobiostratigraphy since the penultimate Glacial (the last 145,000 years) and Ecobioevent Traceability. Mar. Micropaleontol. 115, 24–38.

Dimiza, M.D., Triantaphyllou, M.V., Dermitzakis, M.D., 2008. Seasonality and ecology of living coccolithophores in E. Mediterranean coastal environments (Andros Island, Middle Aegean Sea). Micropaleontology 54, 159–175.

Dimiza, M.D., Triantaphyllou, M.V., Malinverno, E., 2014. New evidence for the ecology of *Helicosphaera carteri* in polluted coastal environments (Elefsis Bay, Saronikos Gulf, Greece). J. Nannoplankton Res. 34, 37–43.

Emeis, K.C., Sakamoto, T., Wehausen, R., Brumsack, H.J., 2000. The sapropel record of the Eastern Mediterranean Sea — results of Ocean Drilling Program Leg 160. Palaeogeogr. Palaeoclimatol. Palaeoecol. 158, 371–395.

Faegri, K., Iversen, J., 1989. Textbook of Pollen Analysis. John Willey & Sons 328.

Faure, G., 1977. Principles of Isotope Geology. John Wiley & Sons, New York 464.

Flores, J.A., Sierro, F.J., Glaçon, G., 1992. Calcareous plankton analysis in the pre-evaporitic sediments of the ODP site 654 (Tyrrhenian Sea, Western Mediterranean). Micropaleontology 38, 279–288.

Flores, J.A., Sierro, F.J., Filippelli, G.M., Bárcena, M.A., Pérez-Folgado, M., Vázquez, A., Utrilla, R., 2005. Surface water dynamics and phytoplankton communities during deposition of cyclic late Messinian sapropel sequences in the western Mediterranean. Mar. Micropaleontol. 56, 50–79.

Flower, B.P., 1999. Data report: planktonic foraminifers from the subpolar North Atlantic and Nordic Seas: sites 980–987 and 907. In: Raymo, M.E., Jansen, E., Blum, P., Herbert, T.D. (Eds.), Proc. ODP, Sci. Results, 162. Ocean Drilling Program, College Station, TX.

Flower, B.P., Kennett, J.P., 1994. The middle Miocene climatic transition — East Antarctic ice-sheet development, deep-ocean circulation and global carbon cycling. Palaeogeogr. Palaeoclimatol. Palaeoecol. 108, 537–555.

Fornaciari, E., Rio, D., 1996. Latest Oligocene to middle Miocene quantitative calcareous nannofossil biostratigraphy in the mediterranean region. Micropaleontology 42, 1–36.

Fornaciari, E., Di Stefano, A., Rio, D., Negri, A., 1996. Middle Miocene quantitative calcareous nannofossil biostratigraphy in the Mediterranean region. Micropaleontology 42, 37–63.

Gartner, S., 1988. Paleoceanography of the mid-Pleistocene. Mar. Micropaleontol. 13, 23–46.

Gibbs, S., Shackleton, N., Young, J., 2004. Orbitally forced climate signals in mid-Pliocene nannofossil assemblages. Marine Micropalaeontology 51, 39–56.

Giunta, S., Negri, A., Morigi, C., Capotondi, L., Combourieu-Nebout, N., Emeis, K.-C., Sangiorgi, F., Vigliotti, L., 2003. Coccolithiphorid ecostratigraphy and multiproxy paleoceanographic reconstruction in the Southern Adriatic Sea during the last deglacial time (Core AD91-17. Palaeogeogr. Palaeoclimatol. Palaeoecol. 190, 39–59.

Gogou, A., Bouloubassi, I., Lykousis, V., Arnaboldi, M., Gaitani, P., Meyers, P.A., 2007. Organic geochemical evidence of abrupt late Glacial-Holocene climate changes in the North Aegean Sea. Palaeogeogr. Palaeoclimatol. Palaeoecol. 256, 1–20.

Grelaud, M., Marino, G., Ziveri, P., Rohling, E.J., 2012. Abrupt shoaling of the nutricline in response to massive freshwater flooding at the onset of the last interglacial sapropel event. Paleoceanography 27 https://doi.org/10.1029/2012PA002288 PA3208.

Hadjistavrinou, Y., 1974. Annual Report of Geological Survey Department of Cyprus, 1973. .

Hagino, K., Okada, H., 2006. Intra- and infra-specific morphological variation in selected coccolithophore species in the equatorial and subequatorial Pacific Ocean. Mar. Micropalaeontol. 58, 184–206.

Haq, B.U., 1980. Biogeographic history of Miocene calcareous nannoplankton and palaeoceanography of the Atlantic Ocean. Micropalaeontology 26, 414–443.

Harrison, R.W., Newell, W.L., Batihanli, H., Panayides, I., McGeehin, J.P., Mahan, S.A., Őzhűr, A., Tsiolakis, E., Necdet, M., 2004. Tectonic framework and Late Cenozoic tectonic history of the northern part of Cyprus: implications for earthquake hazards and regional tectonics. J. Asian Earth Sci. 23, 191–210.

Hilgen, F.J., Abdul Aziz, H., Krijgsman, W., Raffi, I., Turco, E., 2003. Integrated stratigraphy and astronomical tuning of the Serravallian and lower Tortonian at Monte dei Corvi (Middle–Upper Miocene, northern Italy). Palaeogeogr. Palaeoclimatol. Palaeoecol. 199, 229–264.

Holbourn, A., Kuhnt, W., Schulz, M., Flores, J.A., Andersen, N., 2007. Orbitally-paced climate evolution during the middle Miocene "Monterey" carbon-isotope excursion. Earth Planet. Sci. Lett. 261, 534–550.

Hüsing, S.K., Hilgen, F.J., Kuiper, K.F., Krijgsman, W., Turco, E., Cascella, A., Wilson, D., 2010. Astrochronology of the Mediterranean Langhian between 15.29 and 14.17 Ma. Earth Planet. Sci. Lett. 290, 254–269.

Iaccarino, S.M., Di Stefano, A., Foresi, L.M., Turco, E., Baldassini, N., Cascella, A., Da Prato, S., Ferraro, L., Gennari, R., Hilgen, F.J., Lirer, F., Maniscalco, R., Mazzei, R., Riforgiato, F., Russo, B., Sagnotti, L., Salvatorini, G., Speranza, F., Verducci, M., 2011. High-resolution integrated stratigraphy of the upper Burdigalian-lower Langhian in the Mediterranean: the Langhian historical stratotype and new candidate sections for defining its GSSP. Stratigraphy 8, 199–215.

IPCC, 2013. In: Stocker, T.F. (Ed.), IPCC Working Group I Contribution to the IPCC Fifth Assessment Report: Climate Change. Cambridge Univ Press, Cambridge, UK p. 1055.
Jacobs, E., Weissert, H., Shields, G., 1996. The Monterey event in the Mediterranean: a record from shelf sediments of Malta. Paleoceanography 11, 717–728.
John, C.M., Mutti, M., Adatte, T., 2003. Mixed carbonate-siliciclastic record on the North African margin (Malta)—coupling of weathering processes and mid Miocene climate. Geol. Soc. Am. Bull. 115, 217–229.
John, C.M., Karner, G.D., Browning, E., Leckie, R.M., Mateo, Z., Carson, B., Lowery, C., 2011. Timing and magnitude of Miocene eustasy derived from the mixed siliciclastic-carbonate stratigraphic record of the north-eastern Australian margin. Earth Planet. Sci. Lett. 304, 455–467.
Kameo, K., Sato, T., 2000. Biogeography of Neogene calcareous nannofossils in the Caribbean and the eastern equatorial Pacific–Floral response to the emergence of the Isthmus of Panama. Mar. Micropaleontol. 39, 201–218.
Kocsis, L., Vennemann, T.W., Fontignie, D., Baumgartner, C., Montanari, A., Jelen, B., 2008. Oceanographic and climatic evolution of the Miocene Mediterranean deduced from Nd, Sr, C, and O isotope compositions of marine fossils and sediments. Paleoceanography 23 https://doi.org/10.1029/2007PA001540 PA4211.
Kouli, K., Gogou, A., Bouloubassi, I., Triantaphyllou, M.V., Ioakim, C., Katsouras, G., Roussakis, G., Lykousis, V., 2012. Late postglacial paleoenvironmental change in the northeastern Mediterranean region: combined palynological and molecular biomarker evidence. Quat. Int. 261, 118–127.
Kurschner, W., Kvacek, Z., 2009. Oligocene-Miocene CO_2 fluctuations, climatic and palaeofloristic trends inferred from fossil plant assemblages in central Europe. Bull. Geosci. 189–202.
Lirer, F., Foresi, L.M., Iaccarino, S.M., Salvatorini, G., Turco, E., Cosentino, C., Sierro, F.J., Caruso, A., 2019. Mediterranean Neogene planktonic foraminifer biozonation and biochronology. Earth. Rev. 196, 102869. https://doi.org/10.1016/j.earscirev.2019.05.013.
Lohmann, G.P., Carlson, J.J., 1981. Oceanographic significance of Pacific late Miocene calcareous nannoplankton. Mar. Micropaleontol. 6, 553–579.
Lord, R.A., Harrison, R.W., BouDagher-Fadel, M., Stone, B.D., Varol, O., 2009. Miocene mass transport sediments, Troodos Massif, Cyprus. Proc. Geol. Assoc. 120, 133–138.
Lourens, L.J., Hilgen, F.J., Gudjonsson, L., Zachariasse, W.J., 1992. Late Pliocene to Early Pleistocene astronomically forced sea surface productivity and temperature variations in the Mediterranean. Mar. Micropaleontol. 19, 49–78.
Lourens, L.J., Hilgen, F.J., Shackleton, N.J., Laskar, J., Wilson, D., 2004. The Neogene period. In: Gradstein, F.M., Ogg, J.G., Smith, A.G. (Eds.), A Geological Time Scale 2004. Cambridge University Press, pp. 409–440.
Lu, H., Zhang, F., Liu, X., Duce, R.A., 2004. Periodicities of paleoclimatic variations recorded by loess-paleosol sequences in China. Quat. Sci. Rev. 23, 1891–1900.
Malinverno, E., Triantaphyllou, M.V., Stavrakakis, S., Ziveri, P., Lykousis, V., 2009. Seasonal and spatial variability of coccolithophore export production at the South-Western margin of Crete (Eastern Mediterranean). Mar. Micropaleontol. 71, 131–147.
Mantis, M., 1970. Upper cretaceous — tertiary foraminiferal zones in Cyprus. Scientific Research Center of Cyprus, Epetiris 3, 227–241.
Manzi, V., Lugli, S., Roveri, M., Dela Pierre, F., Gennari, R., Lozar, F., Natalicchio, M., Schreiber, B.C., Taviani, M., Turco, E., 2014. The Messinian salinity crisis in Cyprus: a further step towards a new stratigraphic framework for Eastern Mediterranean. Basin Res. 1–30.
Mariotti, A., Dell'Aquila, A., 2012. Decadal climate variability in the Mediterranean region: roles of large-scale forcings and regional processes. Clim. Dyn. 38, 1129–1145.
Martini, E., 1971. Standard tertiary and quaternary calcareous nannoplankton zonation. In: Farinacci, A. (Ed.), Proceedings of the Second Planktonic Conference (Rome) Technoscienza, , pp. 739–785.
Marullo, S., Artale, V., Santoleri, R., 2011. The SST multidecadal variability in the Atlantic-Mediterranean region and its relation to AMO. J. Clim. 24, 4385–4401.
Miller, K.G., Feigenson, M.D., Wright, J.D., Clement, B.M., 1991. Miocene isotope reference section, Deep Sea Drilling Project Site 608: an evaluation of isotope and biostratigraphic resolution. Paleoceanography 6, 33–52.
Miller, K.G., Mountain, G.S., Browning, J.V., Kominz, M., Sugarman, P.J., Christie-Blick, N., Katz, M.E., Wright, J.D., 1998. Cenozoic global sea level, sequences, and the New Jersey Transect: results from coastal plain and continental slope drilling. Rev. Geophys. 36, 569–601.
Mitchel, R.N., Bice, D.M., Montanari, A., Cleaveland, L.C., Christianson, K.T., Coccioni, R., Hinnov, L.A., 2008. Oceanic anoxic cycles? Orbital prelude to the Bonarelli Level (OAE 2). Earth Planet. Sci. Lett. 267, 1–16.
Mourik, A.A., Bijkerk, J.F., Cascella, A., Hüsing, S.K., Hilgen, F.J., Lourens, L.J., Turco, E., 2010. Astronomical tuning of the La Vedova High Cliff Section (Ancona, Italy) — implications of the Middle Miocene Climate Transition for Mediterranean sapropel formation. Earth Planet. Sci. Lett. 297, 249–261.
Mourik, A.A., Abels, H.A., Hilgen, F.J., Di Stefano, A., Zachariasse, W.J., 2011. Improved astronomical age constraints for the middle Miocene climate transition based on high-resolution stable isotope records from the central Mediterranean Maltese Islands. Paleoceanography 26 https://doi.org/10.1029/2010PA001981 PA1210.
Negri, A., Giunta, S., Hilgen, F., Krjigsman, W., Vai, G.B., 1999. Calcareous nannofossil biostratigraphy of the M. del Casino section (northern Apennines, Italy) and paleoceanographic conditions at times of Late Miocene sapropel formation. Mar. Micropaleontol. 36, 13–30.
Negri, A., Cobianchi, M., Luciani, V., Fraboni, R., Milani, A., Claps, M., 2003. Tethyan Cenomanian pelagic rhythmic sedimentation and Pleistocene Mediterranean sapropels: is the biotic signal comparable? Palaeogeogr. Palaeoclimatol. Palaeoecol. 190, 373–397.
Nijenhuis, I., Schenau, S., Van Der Weijden, C., Hilgen, F., Lourens, L., Zachariasse, J.W., 1996. On the origin of upper Miocene sapropelites: a case study from the Faneromeni section, Crete (Greece). Paleoceanography 11, 633–645.
Pagani, M., Zachos, J.C., Freeman, K.H., Tipple, B., Bohaty, S.M., 2005. Marked decline in atmospheric carbon dioxide concentrations during the Paleogene. Science 309, 600–603.
Paul, A., Mulitza, S., Pätzold, J., Wolff, T., 1999. Simulation of oxygen isotopes in a global ocean model. In: Fischer, G., Wefer, G. (Eds.), Use of Proxies in Paleoceanography. Springer-Verlag, Berlin, pp. 655–686.
Payne, A.S., Robertson, A.H.F., 1995. Neogene supra-subduction zone extension in the Polis graben system, west Cyprus. J. Geolog. Soc. London 152, 613–628.
Perch-Nielsen, K., 1985. Cenozoic calcareous nannofossils. In: Bolli, H.M., Saunders, J.B., Perch-Nielsen, K. (Eds.), Plankton Stratigraphy. Cambridge University Press, pp. 427–555.
Press, W.H., Teukolsky, S.A., Vetterling, W.T., Flannery, B.P., 1992. Numerical Recipes in C. Cambridge University Press.
Quaijtaal, W., Donders, T.H., Persico, D., Louwye, S., 2014. Characterising the middle Miocene Mievents in the Eastern North Atlantic realm: a first high-resolution marine palynological record from the Porcupine Basin. Palaeogeogr. Palaeoclimatol. Palaeoecol. 399, 140–159.
Reuter, M., Piller, W.E., Brandano, M., Harzhauser, M., 2013. Correlating Mediterranean shallow water deposits with global Oligocene–Miocene stratigraphy and oceanic events. Glob. Planet. Change 111, 226–236.
Robertson, A.H.F., Eaton, S., Follows, E.J., McCallum, J.E., 1991. The role of local tectonics versus global sea-level change in the Neogene (Miocene-Pliocene) evolution of the Cyprus active margin. In: MacDonald, D.I.M. (Ed.), Sedimentation, Tectonics and Eustacy, 12. Int. Assoc. Sedimentol., Spec. Publ., pp. 331–372.
Rohling, E.J., 1994. Review and new aspects concerning the formation of Mediterranean sapropels. Mar. Geol. 122, 1–28.
Rohling, E., Cane, T.R., Cooke, S., Sprovieri, M., Bouloubassi, I., Emeis, K.-C., Schiebel, R., Kroon, D., Jorissen, F.J., Lorre, A., Kemp, A.E.S., 2002. African monsoon variability during the previous interglacial maximum. Earth Planet. Sci. Lett. 202, 61–75.
Rohling, E.J., Marino, G., Grant, K.M., 2015. Mediterranean climate and oceanography, and the periodic development of anoxic events (sapropels). Earth. Rev. 143, 62–97.
Rossignol-Strick, M., 1985. Mediterranean Quaternary sapropels, an immediate response of the African monsoon to variations of insolation. Palaeogeogr. Palaeoclimatol. Palaeoecol. 49, 237–263.
Shevenell, A.E., Kennett, J.P., Lea, D.W., 2004. Middle Miocene Southern Ocean cooling and Antarctic cryosphere expansion. Science 305, 1766–1770.
Sierro, F.J., Flores, J.C., Francés, G., Vazquez, A., Utrilla, R., Zamarrenõ, I., Erlenkeuser, H., Barcena, M.A., 2003. Orbitally-controlled oscillations in planktic communities and cyclic changes in Western Mediterranean hydrography during the Messinian. Palaeogeogr. Palaeoclimatol. Palaeoecol. 190, 289–316.
Skliris, N., Sofianos, S., Gkanasos, A., Mantziafou, A., Vervatis, V., Axaopoulos, P., Lascaratos, A., 2012. Decadal scale variability of sea surface temperature in the Mediterranean Sea in relation to atmospheric variability. Ocean Dyn. 62, 13–30.
Smith, A.B., Gale, A.S., 2009. The pre-Messinian deep-sea Neogene echinoid fauna of the Mediterranean: surface productivity controls and biogeographical relationships. Palaeogeogr. Palaeoclimatol. Palaeoecol. 281, 115–125.
Sprovieri, R., Bonomo, S., Caruso, A., Di Stefano, A., Di Stefano, E., Foresi, L.M., Iaccarino, S.M., Lirer, F., Mazzei, R., Salvatorini, G., 2002. An integrated calcareous plankton biostratigraphic scheme and biochronology for the Mediterranean Middle Miocene. Rivista Italiana di Paleontologia e Stratigrafia 108, 337–353.
Taylforth, J.E., McCay, G.A., Ellam, R., Raffi, I., Kroon, D., Robertson, A.H.F., 2014. Middle Miocene (Langhian) sapropel formation in the easternmost Mediterranean deep-water basin: evidence from northern Cyprus. Mar. Pet. Geol. 57, 521–536.
Tian, J., Shevenell, A., Wang, P., Zhao, Q., Li, Q., Cheng, X., 2009. Reorganization of pacific deep waters linked to middle Miocene Antarctic cryosphere expansion: a perspective from the South China Sea. Palaeogeogr. Palaeoclimatol. Palaeoecol. 284, 375–382.
Tian, J., Yang, M., Lyle, M.W., Wilkens, R., Shackford, J.K., 2013. Obliquity and long eccentricity pacing of the Middle Miocene climate transition. Geochem. Geophys. Geosystems 14, 1740–1755.
Triantaphyllou, M.V., 2010. Calcareous nannofossil biostratigraphy of Langhian deposits in Lefkas (Ionian Islands). Proceedings of the 12th International Congress, Patras, May, 2010, Bulletin of the Geological Society of Greece XLIII(2) 754–762.
Triantaphyllou, M.V., 2014. Coccolithophore assemblages during the Holocene Climatic Optimum in the NE Mediterranean (Aegean and northern Levantine Seas, Greece): paleoceanographic and paleoclimatic implications. Quat. Int. 345, 56–67.
Triantaphyllou, M.V., Ziveri, P., Tselepides, A., 2004. Coccolithophore export production and response to seasonal surface water variability in the oligotrophic Cretan Sea (NE Mediterranean). Micropaleontology 50, 127–144.
Triantaphyllou, M.V., Ziveri, P., Gogou, A., Marino, G., Lykousis, V., Bouloubassi, I., Emeis, K.-C., Kouli, K., Dimiza, M., Rosell-Mele, A., Papanikolaou, M., Katsouras, G., Nunezm, N., 2009. Late Glacial Holocene climate variability at the south-eastern margin of the Aegean Sea. Mar. Geol. 266, 182–197.
Triantaphyllou, M.V., Antonarakou, A., Dimiza, M., Anagnostou, Ch, 2010. Calcareous nannofossil and planktonic foraminiferal distributional patterns during deposition of sapropels S6, S5 and S1 in the Libyan Sea (Eastern Mediterranean). Geo-marine Lett. 30, 1–13.
Triantaphyllou, M.V., Gogou, A., Dimiza, M.D., Kostopoulou, S., Parinos, K., Rousakis, G., Geraga, M., Bouloubassi, I., Fleitmann, D., Zervakis, V., Velaoras, D., Diamantopoulou, A., Sampatakaki, A., Lykousis, V., 2016. Holocene Climatic Optimum decadal-scale paleoceanography in the NE Aegean (Mediterranean Sea). Geo-marine Lett. 31, 51–66.
Turco, E., Hilgen, F.J., Lourens, L.J., Shackleton, N.J., Zachariasse, W.J., 2001. Punctuated evolution of global climate cooling during the late middle to early late Miocene: high-resolution planktonic foraminiferal and oxygen isotope records from the Mediterranean. Paleoceanography 16, 405–423.

Van Geel, B., Coope, G.R., van der Hammen, T., 1989. Palaeoecology and stratigraphy of the Lateglacial type section at Usselo (The Netherlands). Rev. Palaeobot. Palynol. 60, 25–129.
Vázquez, A., Utrilla, R., Zamarrennõ, I., Sierro, F.J., Flores, J.A., Francés, G., 2000. Precession-related sapropels of the Messinian Sorbas Basin (south Spain): paleoenvironmental significance. Palaeogeogr. Palaeoclimatol. Palaeoecol. 158, 353–370.
Verardo, D.J., Froelich, P.N., McIntyre, A., 1990. Determination of organic carbon and nitrogen in marine sediments using the Carlo Erba NA-1500 Analyser. Deep-Sea Res. 37, 157–216.
Vincent, E., Berger, W.H., 1985. Carbon dioxide and polar cooling in the Miocene: the Monterey hypothesis. In: Sundquisatnd, E.T., Broecker, W.S. (Eds.), The Carbon Cycle and Atmospheric CO2: Natural Variations Archean to Present, Geophys. Monogr. Ser., 32. AGU, Washington D.C, pp. 455–468.
Wade, B.S., Bown, P.R., 2006. Calcareous nannofossils in extreme environments: the Messinian salinity Crisis, Polemi Basin, Cyprus. Palaeogeogr. Palaeoclimatol. Palaeoecol. 233, 271–286.
Westerhold, Th., Marwan, N., Drury, A.J., Liebrand, D., Agnini, C., Anagnostou, E., Barnet, J.S.K., Bohaty, S.M., De Vleeschouwer, D., Florindo, F., Frederichs, Th., Hodell, D.A., Holbourn, A.E., Kroon, D., Lauretano, V., Littler, K., Lourens, L.J., Lyle, M., Pälike, H., Röhl, U., Tian, J., Wilkens, R.H., Wilson, P.A., Zachos, J.C., 2020. An astronomically dated record of Earth's climate and its predictability over the last 66 million years. Science 369, 1383–1387.
Woodruff, F., Savin, S.M., 1985. $\delta^{13}C$ values of Miocene Pacific benthic foraminifera: correlations with sea level and biological productivity. Geology 3, 119–122.
Woodruff, F., Savin, S.M., 1991. Mid-Miocene isotope stratigraphy in the deep sea: high resolution correlations, paleoclimatic cycles, and sediment preservation. Paleoceanography 6, 755–806.
Wright, J.D., Miller, K.G., 1992. Miocene stable isotope stratigraphy, Site 747, Kerguelen Plateau. Proc. Ocean Drill. Prog. Sci. Results 120, 855–866.
Zachos, J.C., Lohmann, K.C., Walker, J.C., Wise, S.W., 1993. Abrupt climate change and transient climates during the Paleogene: a marine perspective. J. Geol. 101, 191–213.
Zachos, J., Pagani, M., Sloan, L., Thomas, E., Billups, K., 2001. Trends, rhythms, and aberrations in global climate 65 Ma to present. Science 292, 686–693.
Zachos, J.C., Dickens, G.R., Zeebe, R.E., 2008. An early Cenozoic perspective on greenhouse warming and carbon-cycle dynamics. Nature 451, 279–283.
Ziveri, P., Baumann, K.H., Böckel, B., Bollmann, J., Young, J., 2004. Biogeography of selected coccolithophores in the Atlantic Ocean, from Holocene sediments. In: Thierstein, H., Young, J. (Eds.), Coccolithophores: From Molecular Processes to Global Impact. Springer Verlag, pp. 403–428.